ADVANCED SUSTAINABLE SYSTEMS
www.advsustainsys.com

# Unveiling the Geometric Site Dependence of Co-Based Spinel Oxides in the Halogen Evolution Reaction

*Chen Chen, Tingting Liu,* Zonghua Pu,* Zhangsen Chen, Xiaofeng Zhang, Qiufeng Huang, Abdullah M. Al-Enizi, Ayman Nafady, Gaixia Zhang,* and Shuhui Sun**

**Cobalt-based spinel oxides, such as $Co_3O_4$, have emerged as promising electrocatalysts for chlorine and bromine evolution reactions (CER and BrER) in recent years. However, the role of Co valence in determining the exceptional performance of $Co_3O_4$ for both CER and BrER remains ambiguous due to the coexistence of both octahedrally coordinated $Co^{3+}$ ($Co^{3+}{}_{Oh}$) and tetrahedrally coordinated $Co^{2+}$ ($Co^{2+}{}_{Td}$) sites, despite their high catalytic activity and stability. Herein, combining experiment results and electrochemical data analysis, the $Co^{3+}{}_{Oh}$ site functions as the primary active site for CER is demonstrated. In contrast, for BrER, both $Co^{3+}{}_{Oh}$ and $Co^{2+}{}_{Td}$ sites exhibit good catalytic activity, with $Co^{3+}{}_{Oh}$ sites displaying better BrER catalytic performance than $Co^{2+}{}_{Td}$ sites. To further enhance the CER catalytic activity of the $Co^{3+}{}_{Oh}$ site, inert $Co^{2+}{}_{Td}$ is replaced with $Cu^{2+}$ cations. As expected, $CuCo_2O_4$ featuring an optimized $Co^{3+}{}_{Oh}$ site demonstrates an overpotential of 24 mV at a current density of 10 mA $cm^{-2}$ while exhibiting exceptional stability for ≈60 h, surpassing the performance of the majority of non-noble and even noble metal-based electrocatalysts reported to date. Therefore, the study elucidates the significance of geometric configuration-dependent activity in electrocatalytic halogen evolution reactions.**

## 1. Introduction

Halogen, particularly chlorine ($Cl_2$) and bromine ($Br_2$), is widely utilized as a fundamental chemical in the synthesis of polymers, pharmaceuticals, dyes, and other related industries.[1–4] The electrolysis of saline water under highly acidic conditions (pH ~2) facilitates efficient chlorine evolution reaction (CER) at the anode, offering a feasible approach for large-scale $Cl_2$ production in an industrial setting.[5–7] In this case, the rational design of an anode electrocatalyst with high activity, selectivity, and stability plays a pivotal role in addressing energy challenges as electrode materials significantly influence both chlorine yield and the overall power consumption of the system. To date, noble-metal-based Ru/Ir oxides have emerged as the predominant electrocatalysts for industrial CER.[8–10] However, the widespread application of these materials has been hindered by their high cost and limited availability of earth-abundant resources.[11–13] Consequently, it is imperative to develop efficient anodes for the CER process by utilizing elements that are more abundant.

In recent years, a series of transition metal, low-noble metal, and non-metal materials have been reported as highly active and stable electrocatalysts for CER. These encompass Ni/Co/Mn-based antimonates,[12,14] Co-based metal oxides,[13,15–17] noble metal (Pt, Ir, etc.)-based single atoms,[5,18,19] and even organic molecules.[20,21] It is worth noting that the cost-effectiveness and exceptional catalytic activities of $Co_3O_4$ have garnered significant attention in the field of catalysis for CER. However, most of these studies primarily focus on enhancing catalytic activity and stability by manipulation of crystallinity, morphology, structure, oxygen vacancies, etc.[13,15–17] In general, the electrocatalytic activity of $Co_3O_4$ is predominantly influenced by the specific geometric arrangement of its sites. This is due to the presence of two octahedrally coordinated $Co^{3+}$

C. Chen, T. Liu, Z. Pu, X. Zhang, Q. Huang
College of Chemistry & Materials Science
Fujian Normal University
Fuzhou, Fujian 350117, China
E-mail: tingtingliu@fjnu.edu.cn; zonghua.pu@fjnu.edu.cn

The ORCID identification number(s) for the author(s) of this article can be found under https://doi.org/10.1002/adsu.202400551



DOI: 10.1002/adsu.202400551

Z. Chen, S. Sun
Institut National de la Recherche Scientifique (INRS)
Centre Énergie Matériaux Télécommunications
Varennes, Québec J3X1P7, Canada
E-mail: shuhui.sun@inrs.ca

A. M. Al-Enizi, A. Nafady
Department of Chemistry
College of Science
King Saud University
Riyadh 11451, Saudi Arabia

G. Zhang
Department of Electrical Engineering
École de Technologie Supérieure (ÉTS)
Montreal, Québec H3C 1K3, Canada
E-mail: gaixia.zhang@etsmtl.ca

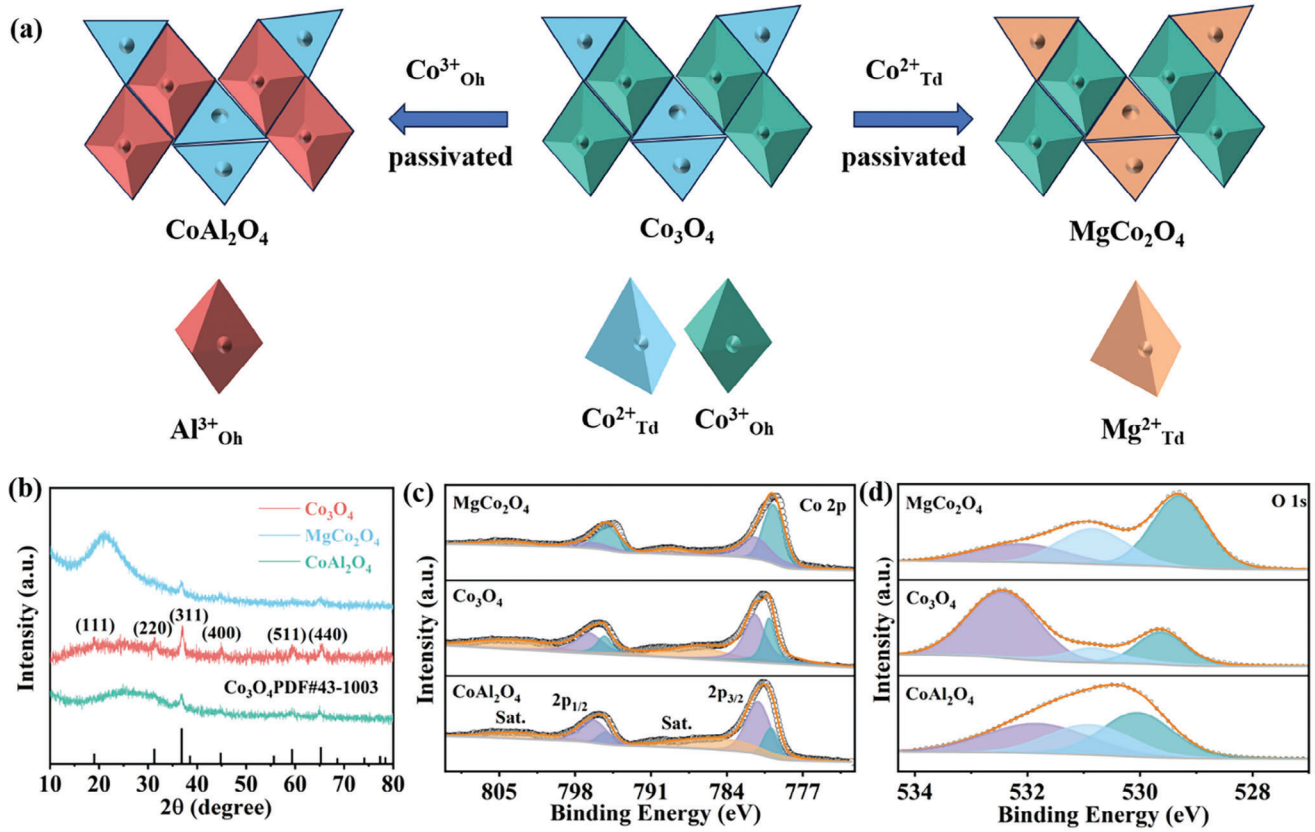


**Figure 1.** a) Schematic illustration of spinel structures of $Co_3O_4$, $CoAl_2O_4$, and $MgCo_2O_4$. b) XRD patterns of $Co_3O_4$, $CoAl_2O_4$, and $MgCo_2O_4$. XPS spectra of c) Co 2p and d) O 1s for $MgCo_2O_4$, $Co_3O_4$, and $CoAl_2O_4$.

($Co^{3+}_{Oh}$) sites and one tetrahedrally coordinated $Co^{2+}$ ($Co^{2+}_{Td}$) site within $Co_3O_4$.[22] For instance, it has been reported that the catalytic activity of $Co_3O_4$ in the oxygen evolution reaction (OER) primarily comes from the $Co^{2+}_{Td}$ site, whereas the oxidation of 5-hydroxymethylfurfural is predominantly facilitated by the $Co^{3+}_{Oh}$ active site.[23,24] Based the $Co_3O_4$ exhibited high activities in important industrial reactions involving chlorine/bromine evolution reactions (CER/BrER), while the dependence of electrocatalysts on geometrical site remains unclear. Therefore, it is worthwhile and crucial to investigate the geometrical site dependence to discern the distinct roles of different sites in $Co_3O_4$ for halogen evolution reactions.

Herein, in this work, we aim to establish the relationship between the geometric location and performance by synthesizing and comparing the activities of halogen evolution reactions for $Co_3O_4$, $MgCo_2O_4$, and $CoAl_2O_4$. Specifically, only $Co^{3+}_{Oh}$ and $Co^{2+}_{Td}$ sites are exposed for $MgCo_2O_4$ and $CoAl_2O_4$, respectively (**Figure 1a**). The electrocatalytic CER performance was observed to exhibit the following trend: $Co_3O_4$ > $MgCo_2O_4$ > $CoAl_2O_4$, indicating the pronounced catalytic activity of $Co^{3+}_{Oh}$. Furthermore, the inert $Co^{2+}_{Td}$ has been substituted with $Cu^{2+}$ cations to enhance the CER catalytic activity. As anticipated, the synthesized $CuCo_2O_4$, featuring optimized $Co^{3+}_{Oh}$ sites, exhibits an overpotential of 24 mV at a current density of 10 mA $cm^{-2}$. In contrast, all three materials ($Co_3O_4$, $MgCo_2O_4$, $CoAl_2O_4$) show good electrocatalytic performance for the BrER. Specifically, $Co_3O_4$, $CoAl_2O_4$, and $MgCo_2O_4$ require an overpotential of 334, 353, and 330 mV, respectively, to achieve a current density of 10 mA $cm^{-2}$. In other words, both the $Co^{3+}_{Oh}$ and $Co^{2+}_{Td}$ sites in $Co_3O_4$ contribute significantly to its overall BrER activity. However, it is worth noting that the catalytic performance of the $Co^{3+}_{Oh}$ sites slightly surpassed that of the $Co^{2+}_{Td}$ sites. Undoubtedly, our study elucidates the significance geometric configuration-dependent activity of spinel oxides for both CER and BrER. This investigation paves the way for enhancing the activity of cobalt-based spinel toward halogen evolution reactions by tuning the $Co^{3+}_{Oh}$ and $Co^{2+}_{Td}$ sites.

## 2. Results and Discussion

### 2.1. Synthesis and Characterization of Catalysts

The synthesis of $Co_3O_4$, $MgCo_2O_4$, and $CoAl_2O_4$ was accomplished via a two-step process, involving hydrothermal treatment followed by calcination in air. The substitution of $Mg^{2+}$ and $Al^{3+}$ ions for the tetrahedral and octahedral sites in $Co_3O_4$ led to the formation of $MgCo_2O_4$ and $CoAl_2O_4$ (Figure 1a), respectively. The structure of $Co_3O_4$, $MgCo_2O_4$, and $CoAl_2O_4$ was determined using powder X-ray diffraction (XRD). The observed peaks at $2\theta$ angles of 19.0°, 31.3°, 36.8°, 38.5°, 44.8°, 55.7°, 59.4°, and 65.2° in Figure 1b correspond to the crystal planes (111), (220), (311), (222), (400), (422), (511), and (440), respectively for $Co_3O_4$, $MgCo_2O_4$ and $CoAl_2O_4$ spinels with the identical structure but distinct geometric arrangements of Co sites (Figure 1b).[24] The

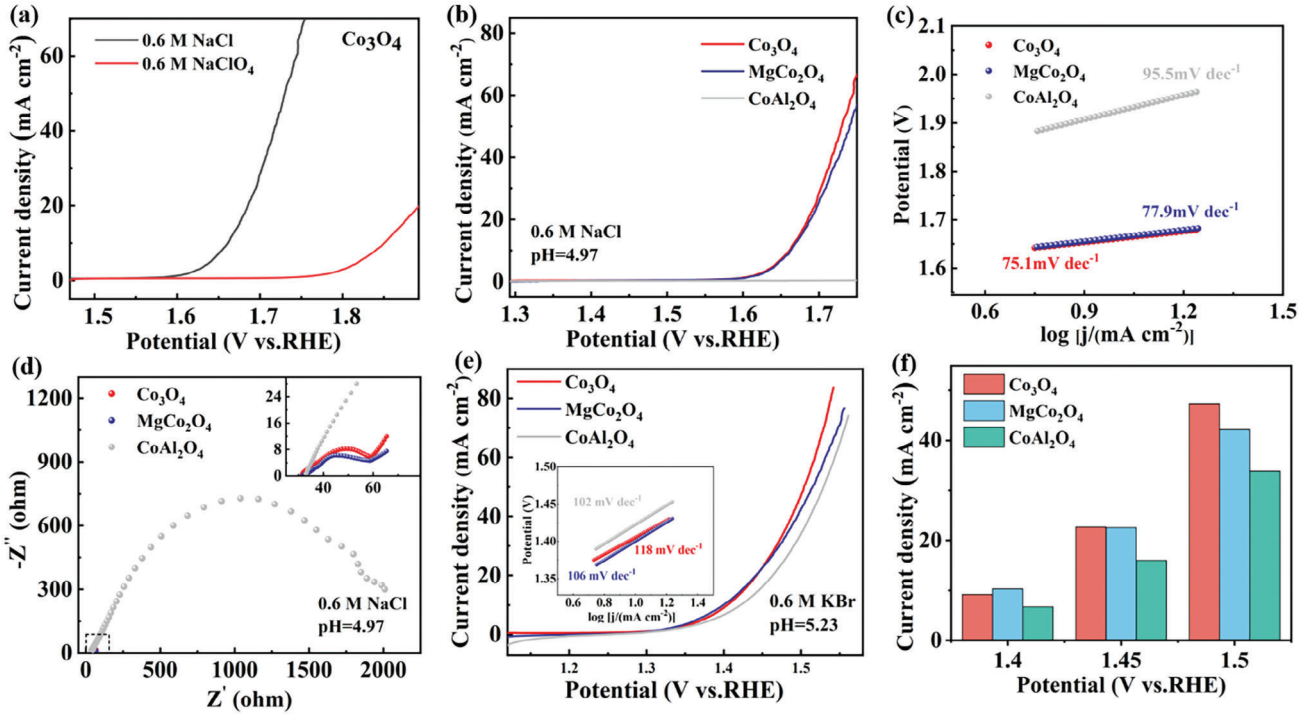


**Figure 2.** a) LSV curves of $Co_3O_4$ in 0.6 M NaCl and $NaClO_4$ solution. b) Polarization curves of $Co_3O_4$, $CoAl_2O_4$, and $MgCo_2O_4$ electrocatalysts in 0.6 M NaCl solution. c) Tafel plots were obtained from the polarization curves in (b). d) Nyquist plots of $Co_3O_4$, $MgCo_2O_4$, and $CoAl_2O_4$ were collected under the same conditions. e) Polarization curves of $Co_3O_4$, $CoAl_2O_4$, and $MgCo_2O_4$ electrocatalysts in 0.6 M KBr solution. f) Corresponding current densities at potential of 1.4, 1.45, and 1.5 V for $Co_3O_4$, $CoAl_2O_4$, and $MgCo_2O_4$ electrocatalysts.

valence state of Co in different spinels was further determined through X-ray photoelectron spectroscopy (XPS) measurements (Figure 1c,d). As illustrated in Figure 1c, the Co 2p spectra in all samples exhibited two distinct peaks corresponding to Co $2p_{1/2}$ and Co $2p_{3/2}$, which are indicative of the spin-orbit bimodal features of Co 2p. The broad Co $2p_{3/2}$ and Co$2p_{1/2}$ peak of $Co_3O_4$ can be further resolved into two distinct peaks for $Co^{2+}$ (781.3 and 796.8 eV) and $Co^{3+}$ species (780.1 and 794.8 eV), respectively. In comparison to $Co_3O_4$ containing both $Co^{2+}$ and $Co^{3+}$, the surfaces of $MgCo_2O_4$ and $CoAl_2O_4$ are predominantly occupied by $Co^{3+}$ and $Co^{2+}$ (Figure S1, Supporting Information), respectively. Therefore, the oxides examined in this study predominantly contain $Co^{3+}$ or $Co^{2+}$ site, or a combination of both, thereby offering valuable insights into the correlation between the geometric configuration of cobalt sites and their catalytic activity. Similarly, the O 1s spectra of $Co_3O_4$, $MgCo_2O_4$, and $CoAl_2O_4$ also exhibit distinct differences. Specifically, as shown in Figure 1d, the O 1s peak of $Co_3O_4$ is observed at a bonding energy of 529.8 eV. Moreover, it is worth noting that in comparison with $CoAl_2O_4$, the O 1s characteristic peak of $MgCo_2O_4$ exhibits a lower binding energy. In other words, the interaction between $Co^{3+}$ and $O^{2-}$ in $MgCo_2O_4$ is stronger than that between $Co^{2+}$ and $O^{2-}$ in $CoAl_2O_4$. Consequently, these structure differences may further impact the catalytic activity in various oxidation and (or) reduction reactions, including water oxidation/reduction, $O_2$ reduction, $N_2/NO_2^-/NO_3^-$ reduction, CER, etc.[25–28] The characterizations provide conclusive evidence for the successful synthesis and characterization of three spinel-type cobalt oxides, namely $Co_3O_4$, $MgCo_2O_4$, and $CoAl_2O_4$.

### 2.2. Evaluating the Catalytic Performance of Cobalt-Based Spinel Oxide Toward Halogen Evolution Reactions

We first assessed the CER performance of $Co_3O_4$, $MgCo_2O_4$, and $CoAl_2O_4$ in 0.6 M NaCl solution. It is worth noting that **Figure 2a** also illustrates linear sweep voltammetry (LSV) of $Co_3O_4$ in 0.6 $NaClO_4$ solutions (pH 8.00, Figure S2, Supporting Information). The selection of $NaClO_4$ as the appropriate electrolyte is based on its suitability attributed to the presence of perchlorate ions ($ClO_4^-$), which are fully oxidized oxyanions of chlorine. In other words, under anodic bias, these anions undergo no further oxidation except for the OER. As shown in Figure 2a, during anodic polarization in the presence of chloride with a concentration of 0.6 M NaCl, the onset potential for $Co_3O_4$ was observed to be ≈1.6 V (vs RHE, black curve), exhibiting a reduction of ≈120 mV (red curve) compared to that recorded without chloride solutions (0.6 M $NaClO_4$). In other words, the observed cathodic shift in the LSV under 0.6 M NaCl implies a significantly enhanced performance of CER over OER in the electrolyte-containing chloride. Furthermore, this value compares favorably with the behaviors of most non-noble, and even noble-metal-based CER catalysts reported to date (Table S1, Supporting Information). Although the high catalytic activity of $Co_3O_4$ has been achieved, the role of Co valence in determining its exceptional performance toward CER remains ambiguous due to the coexistence of both $Co^{3+}{}_{Oh}$ and $Co^{2+}{}_{Td}$ sites. Consequently, the CER performance of $MgCo_2O_4$ and $CoAl_2O_4$, which predominantly consist of $Co^{3+}$ and $Co^{2+}$ sites, was further evaluated in 0.6 M NaCl solution. The comparative performance of the three materials in terms of CER can

be ranked as follows, as depicted in Figure 2b: $Co_3O_4$ exhibits comparable performance to $MgCo_2O_4$, while $CoAl_2O_4$ demonstrates negligible activity. This obtained result suggests that the CER process predominantly occurs at the $Co^{3+}{}_{Oh}$ site, while the catalytic effect of the $Co^{2+}{}_{Td}$ site on CER is relatively weak. Furthermore, the lower Tafel slope of $MgCo_2O_4$ (77.9 mV $dec^{-1}$), in comparison to the $Co^{2+}{}_{Td}$ sites in $CoAl_2O_4$ (95.5 mV $dec^{-1}$), suggests that the presence of $Co^{3+}{}_{Oh}$ sites promotes the CER reaction process and accelerates reaction kinetics (Figure 2c). Subsequently, considering the utility of electrochemical impedance spectroscopy (EIS) as a valuable tool for investigating electrocatalytic reaction kinetics and electrode/electrolyte interface characteristics, we conducted EIS measurements on $Co_3O_4$, $MgCo_2O_4$, and $CoAl_2O_4$ under identical applied potentials to further elucidate the active site of CER. The Nyquist plots in Figure 2d, demonstrate that the charge transfer resistance ($R_{ct}$) of the three samples follows the order $MgCo_2O_4 \approx Co_3O_4 < CoAl_2O_4$. This observation suggests that both $Co_3O_4$ and $MgCo_2O_4$ with a $Co^{3+}{}_{Oh}$ structure exhibit smaller $R_{ct}$ values compared to $CoAl_2O_4$ with a $Co^{2+}{}_{Td}$ structure only. In other words, the presence of $Co^{3+}{}_{Oh}$ in spinel facilitates electron and ion transfer during the CER process. Likewise, the exceptional intrinsic CER activity of $Co^{3+}{}_{Oh}$ was further supported by its superior electrochemical surface area (ECSA). As illustrated in (Figure S3, Supporting Information), the electrochemical double layer capacitance ($C_{dl}$) values of $Co_3O_4$, $MgCo_2O_4$, and $CoAl_2O_4$ were 11.45, 11.24, and 0.96 mF $cm^{-2}$, respectively. This indicates that all three catalysts exhibit comparable ECSAs. Similarly, $Co_3O_4$ and $MgCo_2O_4$ exhibit higher CER activities than $CoAl_2O_4$ in 0.6 M NaCl solution, which provides compelling evidence that the $Co^{3+}{}_{Oh}$ site is the primary active site for CER. Therefore, these findings unveil the different contributions of varying types of cobalt sites to CER.

It is worth noting that the catalytic activities of all three materials ($Co_3O_4$, $MgCo_2O_4$, $CoAl_2O_4$) toward BrER were further examined. As illustrated in Figure 2e, both $Co_3O_4$ and $MgCo_2O_4$, exhibit slightly superior electrocatalytic performance toward BrER compared to $CoAl_2O_4$. Specifically, an overpotential of 334, 353, and 330 mV is required for achieving a current density of 10 mA $cm^{-2}$ for $Co_3O_4$, $CoAl_2O_4$, and $MgCo_2O_4$, respectively. In contrast to CER, the electrocatalytic performance is primarily determined by the $Co^{3+}{}_{Oh}$ sites rather than other sites. In the case of BrER, both $Co^{3+}{}_{Oh}$ and $Co^{2+}{}_{Td}$ sites exhibit favorable catalytic activity; however, the $Co^{3+}{}_{Oh}$ sites demonstrate superior activity in BrER compared to the $Co^{2+}{}_{Td}$ sites (Figure 2f). Additionally, both $Co_3O_4$ and $MgCo_2O_4$ samples exhibit slightly lower Tafel slops than that of $CoAl_2O_4$ (inset of Figure 2e). This result further indicates that $Co^{3+}{}_{Oh}$ possesses higher BrER activity than that of $Co^{2+}{}_{Td}$ sites.

As demonstrated above, the octahedral $Co^{3+}$ sites in spinel oxides have been shown to function as catalytic active sites for both CER and BrER. Therefore, increased exposure to these sites could potentially enhance the electrocatalytic activity for halogen evolution reaction.[29,30] Fortunately, the regulation of specific sites' exposure can be achieved by manipulating the atomic structure of spinel oxides. In comparison to $Mg^{2+}$ and $Co^{2+}$, which occupy octahedral $Co^{3+}$ sites in spinel oxides, $Cu^{2+}$ emerges as a promising candidate for occupying tetrahedral sites due to its distinctive electronic structure ($3d^9 4s^1$).[25] Consequently, the spinel oxides of $CuCo_2O_4$ were further designed to validate this hypothesis. As illustrated in **Figure** 3a, the binding energy of Co $2p_{3/2}$ to $Co^{3+}{}_{oh}$ exhibits an upward shift with Cu doping, indicating that the incorporation of Cu dopants effectively modulates the electronic structure of $Co^{3+}{}_{Oh}$.[3] Therefore, the main role of Cu doping is to enhance the CER activity of $Co^{3+}{}_{Oh}$. Subsequently, the transmission electron microscopy (TEM) image reveals the presence of numerous nanoparticles in the $CuCo_2O_4$ nanomaterials (Figure 3b,c). The high-resolution TEM (HRTEM) image reveals that the interplanar spacing for such nanoparticle was determined as 0.24 nm, which corresponds to the (311) plane of $CuCo_2O_4$ (Figure 3d). More importantly, this is corroborated by the fact that the highest intensity of XRD peaks is found at the (311) surface (Figure S4, Supporting Information).[32–34] Furthermore, the scanning TEM (STEM) and energy dispersive X-ray (EDX) elemental mapping images (Figure 3e–i) provide further evidence of the homogenous distribution of copper, cobalt, and oxygen elements.

Additionally, the CER activity was further evaluated and compared with that of commercially available $RuO_2$ in 0.6 M NaCl electrolyte at room temperature. As evidenced by the LSV curves in **Figure** 4a, $CuCo_2O_4$ exhibits a rapid initiation with a pronounced surge in the anodic current density. In detail, to attain a current density of 10 mA $cm^{-2}$, $CuCo_2O_4$ only needs an overpotential of 24 mV, exhibiting a Tafel slope 71.1 mV $dec^{-1}$, significantly lower than that observed for the commercial $RuO_2$ (28 mV and 78.5 mV $dec^{-1}$) (Figure 4a,b; Figure S5, Supporting Information). Furthermore, this value compares favorably with the behaviors of most Co-based, Pt/Ir/Ru-based CER catalysts reported to date (Figure 4c; Table S1, Supporting Information).[35,36] More importantly, the polarization curves before and after 1000 cyclic voltammetry (CV) cycles are illustrated in Figure 4d. After 1000 CV cycles, the polarization curve for $CuCo_2O_4$ presents almost no degradation. For comparison, commercial $RuO_2$ was also evaluated under identical conditions (Figure S6, Supporting Information). Notably, the LSV of $RuO_2$ exhibits a negative shift of ≈4 and 49 mV after 1000 CV cycles to achieve current densities of 10 and 100 mA $cm^{-2}$, indicating a substantial decline in its performance. Furthermore, chronoamperometry measurement of $CuCo_2O_4$ was conducted at a potential of 1.65 V (without iR-correction). Following a 60 h test, the current density showed negligible degradation, further confirming the good stability of the $CuCo_2O_4$ material (Figure 4e). The excellent durability of $CuCo_2O_4$ following CER testing was further validated through analysis of the XRD pattern. As depicted in Figure S7 (Supporting Information), no significant discrepancies were observed in the XRD patterns before and after the stability assessment. It is noteworthy that the $CuCo_2O_4$ sample also exhibits superior catalytic activity and stability in terms of BrER compared to $Co_3O_4$, $MgCo_2O_4$, and $CoAl_2O_4$ (Figure 4f; Figures S8 and S9, Supporting Information).[37]

## 3. Conclusion

In summary, we have successfully demonstrated the geometrical site-dependent catalytic activity of $Co_3O_4$ spinel oxide for CER and BrER by incorporating $Mg^{2+}$ and $Al^{3+}$ ions into tetrahedral and octahedral sites, respectively. Our study demonstrated that the $Co^{3+}{}_{Oh}$ site functions as the primary active site for CER in spinel $Co_3O_4$. Notably, both $Co^{3+}{}_{Oh}$ and $Co^{2+}{}_{Td}$ sites exhibit good catalytic activity for BrER, but the $Co^{3+}{}_{Oh}$ sites show superior

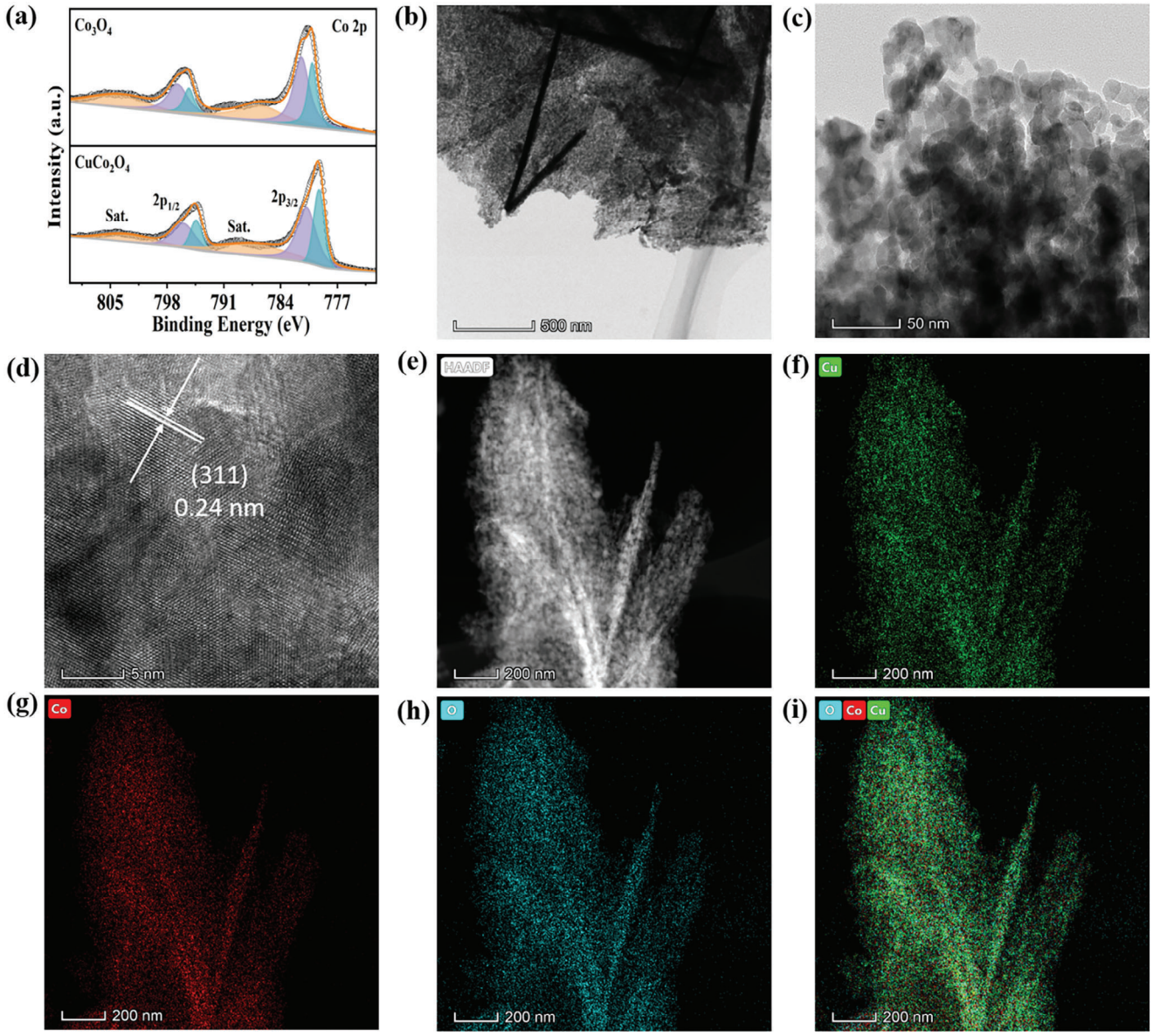


**Figure 3.** a) Co 2p XPS spectra for $CuCo_2O_4$ and $Co_3O_4$. b,c) TEM and d) HRTEM images of $CuCo_2O_4$. e–i) HAADF images and EDX elemental mapping of Cu, Co, and O of $CuCo_2O_4$.

performance compared to the $Co^{2+}{}_{Td}$ sites. To further enhance the catalytic activity of the $Co^{3+}{}_{Oh}$ site, we substituted inert $Co_{Td}{}^{2+}$ with $Cu^{2+}$ cations. As anticipated, $CuCo_2O_4$ featuring optimized $Co^{3+}{}_{Oh}$ sites demonstrate an overpotential of 24 and 330 mV at a current density of 10 mA $cm^{-2}$ toward CER and BrER, respectively. More importantly, the $CuCo_2O_4$ displays a durability of over 60 h for CER. Therefore, this work emphasizes the importance of the geometrical site configuration in spinel $Co_3O_4$ for electrochemical halogen evolution reactions. These findings present a promising avenue for integrating renewable electricity derived from solar or wind, as earth-abundant spine oxide electrocatalysts pave the way toward the environmental-friendly and cost-effective generation of $Cl_2$, $Br_2$, $HClO_4$, $NaClO_4$, and other compounds crucial for wastewater treatment, chemical synthesis, and other significant applications in the future.

## 4. Experimental Section

*Synthesis of $Co_3O_4$*: The synthesis of $Co_3O_4$ was successfully accomplished using the previously reported method.[24] Initially, two solutions were prepared: one containing 0.04 mol of $Na_2CO_3$ and the other containing 0.02 mol of $Co(NO_3)_2$. Subsequently, the two solutions were combined in equal proportions and transferred into a beaker, followed by vigorous stirring. The aforementioned mixture (30 mL) was subsequently transferred to a 50 mL polytetrafluoroethylene reactor and subjected to thermal treatment at 100 °C for 24 h. Upon completion of the reaction, the product was washed thrice with high-purity water and then dried at 60 °C for 10 h. Finally, the precursor underwent annealing in an air environment at 350 °C for a period of 2 h, aiming to obtain the $Co_3O_4$ sample. Similarly, $MgCo_2O_4$, $CoAl_2O_4$, and $CuCo_2O_4$ were synthesized using analogous procedures.

*Characterization*: XRD was conducted using a Shimadzu XRD-6100 diffractometer equipped with Cu K$\alpha$ radiation ($\lambda$ = 0.15418 nm). XPS

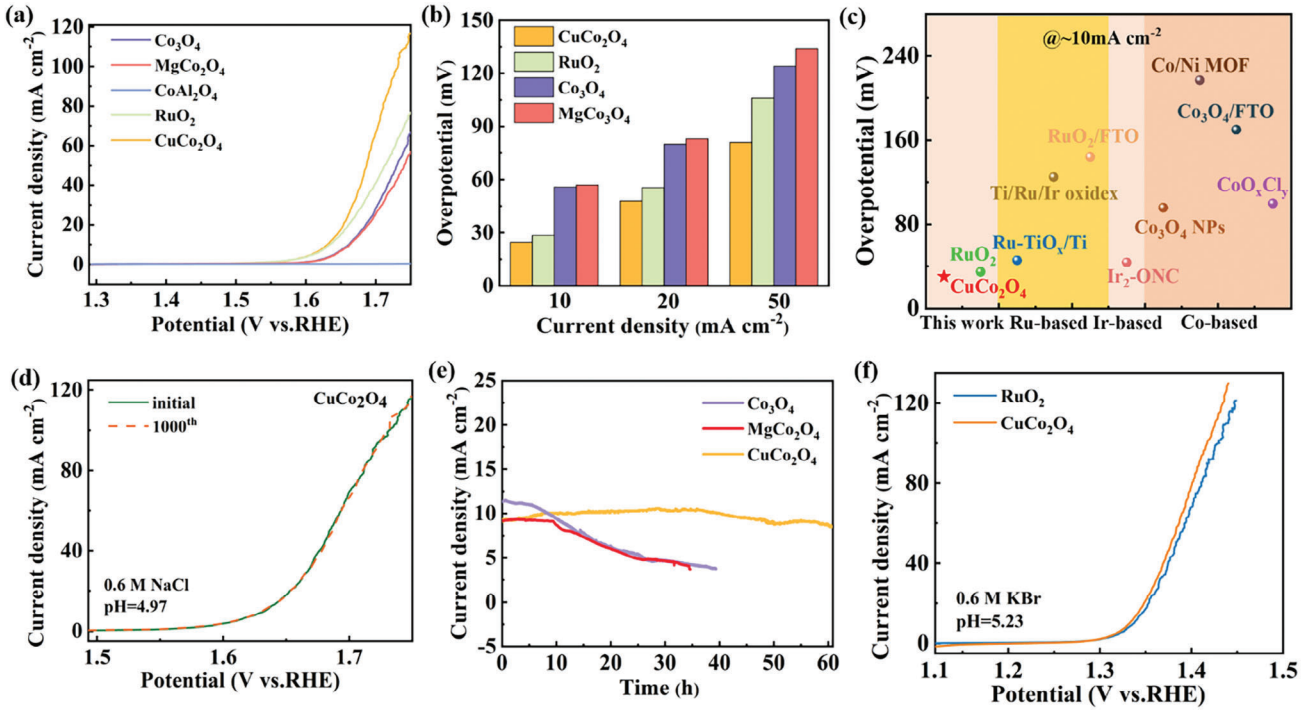


**Figure 4.** (a) The LSV curves of $MgCo_2O_4$, $Co_3O_4$, $CoAl_2O_4$, $CuCo_2O_4$, and $RuO_2$ in 0.6 M NaCl solution. b) Overpotentials of $MgCo_2O_4$, $Co_3O_4$, $CoAl_2O_4$, $CuCo_2O_4$, and $RuO_2$ at different current densities. c) Comparison of overpotential with different representative catalysts. d) Polarization curves were recorded before and after 1000 CV cycles for $CuCo_2O_4$. e) Time-dependent current density curves for $MgCo_2O_4$, $Co_3O_4$, and $CuCo_2O_4$ were measured at potentials in 0.6 M NaCl solution(without iR-correction). f) LSV curves of $RuO_2$ and $CuCo_2O_4$ at 0.6 M KBr solution.

analysis was conducted using a Thermo Scientific K-Alpha XPS spectrometer equipped with a monochromatic Al K$\alpha$ source ($h\nu$ = 1486.6 eV). TEM and corresponding EDX elemental mapping images were observed on a Titan G2 60–300 electron microscope equipped with an EDX spectrometer. The operating voltage was set to 300 kV.

*Electrochemical Measurement*: A catalyst ink was prepared and applied to a 3 mm diameter glassy carbon electrode for testing as a CER or BrER working electrode. Specifically, 5 mg of catalyst was dispersed in a mixture comprising 0.2 mL of water, 0.44 mL of isopropanol, and 10 µl of a 5% Nafion solution. This mixture was then sonicated for half an hour to form the catalyst ink, which was then applied in three coats to the pre-polished glassy carbon electrode. After air-drying, the catalyst loading was ≈0.82 ± 0.03 mg $cm^{-2}$.

All electrochemical performance tests were conducted on an electrochemical workstation (CHI 660E, CH Instrument, Shanghai Chenhua, China). The experimental setup employed a three-electrode system, consisting of a graphite rod and an Ag/AgCl electrode employed as the counter and reference electrode, respectively. The CER and BrER performances of the catalysts were investigated in 0.6 M NaCl (pH 4.97) and 0.6 M KBr (pH 5. 23) (Figure S1, Supporting Information), respectively. All electrochemical measurements were carried out at room temperature (≈25 °C). The potentials were converted to a reversible hydrogen electrode (RHE) reference scale using the following equation.

$$E_{versus\ RHE} = E_{versus\ Ag/AgCl} + 0.197V + \left(\frac{RT\ln 10}{F}\right) pH \quad (1)$$

where R represents the gas constant (8.314 J $K^{-1}$ $mol^{-1}$). T denotes the temperature in Kelvin (K). F is the Faraday constant (96 485 C $mol^{-1}$), respectively. The equilibrium potential of CER ($E_{CER}$) can be obtained by employing the Nernst equation, which incorporates factors such as temperature, chloride ion activity, and chlorine gas partial pressure.

$$E_{CER}\,(T, \alpha\,(Cl_2), \alpha\,(Cl^-))\ versus\ RHE = E^{O}_{CER} - \left(\frac{RT}{F}\right)\ln \alpha\,(Cl^-) + \left(\frac{RT}{2F}\right)\ln \alpha\,(Cl_2) + \left(\frac{RT\ln 10}{F}\right) pH \quad (2)$$

where $E^{\circ}_{CER}$ represents the equilibrium potential of the CER under standard conditions ($E^{\circ}_{CER}$ = 1.358 V vs standard hydrogen electrode (SHE)), $\alpha(Cl_2)$ was assumed to be 0.01, and $\alpha(Cl^-)$ was determined to be 0.6 based on the experimental conditions.[5]

The equilibrium potential in the system was determined to be 1.6 V versus RHE, while the geometric current density of 10 mA $cm^{-2}$ was employed for comparative analysis of overpotentials. EIS was performed using an AC voltage with an amplitude of 5 mV and a frequency range spanning from $10^5$ to 0.1 Hz. Chronoamperometric current measurements were employed for long-term durability experiments. Accelerated durability tests of the catalysts were performed in a solution containing 0.6 M NaCl at room temperature by applying potential cycling between 0.8 and 1.4 V versus Ag/AgCl at a scan rate of 100 mV $s^{-1}$ for a total of 1000 cycles. All presented data were adjusted for RHE using iR compensation, where i represents the current and R denotes the uncompensated electrolyte ohmic resistance measured via EIS.[38–42]

ECSA was investigated through measurements of electrochemical $C_{dl}$. CV measurements were employed to analyze the electrochemical $C_{dl}$, within the range of 0.75–0.95 V relative to the RHE, excluding Faraday current and with a scan rate of 20 to 120 mV $s^{-1}$. The values of the fitted slopes were plotted as $C_{dl}$ by graphing the half difference between anodic and cathodic scanning current densities at a fixed potential ($\Delta j/2$) against the scan rate.[43–46]

## Supporting Information

Supporting Information is available from the Wiley Online Library or from the author.

## Acknowledgements

This work was supported by the Fujian Province Young and Middle-Aged Teacher Education Research Project (JZ230009), A.M.A.-E. and Z.P. extend their sincere appreciation to the Distinguished Scientist Fellowship Program (DSFP) at King Saud University.

## Conflict of Interest

The authors declare no conflict of interest.

## Data Availability Statement

The data that support the findings of this study are available from the corresponding author upon reasonable request.

## Keywords

chlorine/bromine evolution reaction, electrocatalyst, octahedral coordination, spinel oxide

Received: July 30, 2024
Revised: October 16, 2024
Published online:

[1] R. K. B. Karlsson, A. Cornell, *Chem. Rev.* **2016**, *116*, 2982.
[2] J. Yang, W.-H. Li, K. Xu, S. Tan, D. Wang, Y. Li, *Angew. Chem., Int. Ed.* **2022**, *61*, e202200366.
[3] Y. Yao, L. Zhao, J. Dai, J. Wang, C. Fang, G. Zhan, Q. Zheng, W. Hou, L. Zhang, *Angew. Chem., Int. Ed.* **2022**, *61*, e202208215.
[4] Y. Gao, M. Yan, C. Cheng, H. Zhong, B. Zhao, C. Liu, Y. Wu, B. Zhang, *J. Am. Chem. Soc.* **2024**, *146*, 714.
[5] J. Wang, L. Zhao, Y. Zou, J. Dai, Q. Zheng, X. Zou, L. Hu, W. Hou, R. Wang, K. Wang, Y. Shi, G. Zhan, Y. Yao, L. Zhang, *J. Am. Chem. Soc.* **2024**, *146*, 11152.
[6] E. Chlor, *Chlorine Industry Rev.* **2013**, *2014*, 1.
[7] J. Crook, A. Mousavi, *Environ. Forensics* **2016**, *17*, 211.
[8] Y. Wang, Y. Liu, D. Wiley, S. Zhao, Z. Tang, *J. Mater. Chem. A* **2021**, *9*, 18974.
[9] N. Menzel, E. Ortel, K. Mette, R. Kraehnert, P. Strasser, *ACS Catal.* **2013**, *3*, 1324.
[10] S. Choi, W. I. Choi, J. S. Lee, C. H. Lee, M. Balamurugan, A. D. Schwarz, Z. S. Choi, H. Randriamahazaka, K. T. Nam, *Adv. Mater.* **2023**, *35*, 2300429.
[11] Y. Zhao, Z. Niu, J. Zhao, L. Xue, X. Fu, J. Long, *Electrochem. Energy Rev.* **2023**, *6*, 14.
[12] A. Ali, F. Long, P. Shen, *Electrochem. Energy Rev.* **2022**, *5*, 1.
[13] M. Xiao, Q. Wu, R. Ku, L. Zhou, C. Long, J. Liang, A. Mavrič, L. Li, J. Zhu, M. Valant, J. Li, Z. Zeng, C. Cui, *Nat. Commun.* **2023**, *14*, 5356.
[14] H. Dong, X. Shao, S. Hancox, S. T. McBeath, W. A. Tarpeh, M. R. Hoffmann, *ACS Appl. Mater. Interfaces* **2023**, *15*, 40369.
[15] X. Zhu, P. Wang, Z. Wang, Y. Liu, Z. Zheng, Q. Zhang, X. Zhang, Y. Dai, M. Whangbo, B. Huang, *J. Mater. Chem. A* **2018**, *6*, 12718.
[16] H. Ha, K. Jin, S. Park, K. Lee, K. H. Cho, H. Seo, H. Ahn, Y. H. Lee, K. T. Nam, *J. Phys. Chem. Lett.* **2019**, *10*, 1226.
[17] W. I. Choi, S. Choi, M. Balamurugan, S. Park, K. H. Cho, H. Seo, H. Ha, K. T. Nam, *ACS Omega* **2023**, *8*, 35034.
[18] L. Quan, X. Chen, J. Liu, S. Fan, B. Xia, B. You, *Adv. Funct. Mater.* **2023**, *33*, 2307643.
[19] T. Lim, G. Y. Jung, J. H. Kim, S. O. Park, J. Park, Y. Kim, S. J. Kang, H. Y. Jeong, S. K. Kwak, S. H. Joo, *Nat. Commun.* **2020**, *11*, 412.
[20] J. Yang, W. Li, H. Tang, Y. Pan, D. Wang, Y. Li, *Nature* **2023**, *617*, 519.
[21] J. Yang, C. Zhu, D. Wang, *Angew. Chem., Int. Ed.* **2024**, *63*, e202406883.
[22] J. Wu, X. Wang, W. Zheng, Y. Sun, Y. Xie, K. Ma, Z. Zhang, Q. Liao, Z. Tian, Z. Kang, Y. Zhang, *J. Am. Chem. Soc.* **2022**, *144*, 19163.
[23] H. Wang, S. Hung, H. Chen, T. Chan, H. Chen, B. Liu, *J. Am. Chem. Soc.* **2016**, *138*, 36.
[24] Y. Lu, V. Dong, Y. Huang, Y. Zou, Z. Liu, Y. Liu, Y. Li, N. He, J. Shi, S. Wang, *Angew. Chem., Int. Ed.* **2020**, *59*, 19215.
[25] Q. Hu, S. Qi, Q. Huo, Y. Zhao, J. Sun, X. Chen, M. Lv, W. Zhou, C. Feng, X. Chai, H. Yang, C. He, *J. Am. Chem. Soc.* **2023**, *146*, 2967.
[26] T. Wang, Y. Sun, Y. Zhou, S. Sun, X. Hu, Y. Dai, S. Xi, Y. Du, Y. Yang, Z. J. Xu, *ACS Catal.* **2018**, *8*, 8568.
[27] H. Bai, D. Chen, Q. Ma, R. Qin, H. Xu, Y. Zhao, J. Chen, S. Mu, *Electrochem. Energy Rev.* **2022**, *5*, 24.
[28] S. Sun, Y. Sun, Y. Zhou, S. Xi, X. Ren, B. Huang, H. Liao, L. P. Wang, Y. Du, Z. J. Xu, *Angew. Chem., Int. Ed.* **2019**, *58*, 6042.
[29] V. Singh, T. C. Nagaiah, *J. Mater. Chem. A* **2019**, *7*, 10019.
[30] Z. Mao, S. Chen, J. Ji, H. Yin, *Chin. Sci. Bull.* **2024**, *69*, 3748.
[31] Y. Wang, H. Li, W. Zhou, X. Zhang, B. Zhang, Y. Yu, *Angew. Chem., Int. Ed.* **2022**, *61*, e202202604.
[32] H. Jin, P. Li, P. Cui, J. Shi, W. Zhou, X. Yu, W. Song, C. Cao, *Nat. Commun.* **2022**, *13*, 723.
[33] W. Tan, S. Xie, D. Le, W. Diao, M. Wang, K.-B. Low, D. Austin, S. Hong, F. Gao, L. Dong, L. Ma, S. N. Ehrlich, T. S. Rahman, F. Liu, *Nat. Commun.* **2022**, *13*, 7070.
[34] A. R. Zeradjanin, N. Menzel, W. Schuhmann, P. Strasser, *Phys. Chem. Chem. Phys.* **2014**, *16*, 13741.
[35] R. Chen, V. Trieu, A. R. Zeradjanin, H. Natter, D. Teschner, J. Kintrup, A. Bulan, W. Schuhmann, R. Hempelmann, *Phys. Chem. Chem. Phys.* **2012**, *14*, 7392.
[36] Z. Yu, G. Xia, V. M. Diaconescu, L. Simonelli, A. P. LaGrow, Z. Tai, X. Xiang, D. Xiong, L. Liu, *Chem. Sci.* **2024**, *15*, 9216.
[37] D. Jain, J. Hightower, D. Basu, V. Gustin, Q. Zhang, A. C. Co, A. Asthagiri, U. S. Ozkan, *J. Catal.* **2022**, *413*, 1005.
[38] X. Lv, W. Tian, Z. Yuan, *Electrochem. Energy Rev.* **2023**, *6*, 23.
[39] M. Ha, P. Thangavel, N. K. Dang, D. Y. Kim, S. Sultan, J. S. Lee, K. S. Kim, *Small* **2023**, *19*, 2300240.
[40] J. Ji, J. Liu, L. Shi, S. Guo, N. Cheng, P. Liu, Y. Gu, H. Yin, H. Zhang, H. Zhao, *Small Struct.* **2024**, *5*, 2300240.
[41] L. Zhang, J. Liang, X. He, Q. Yang, Y. Luo, D. Zheng, S. Sun, J. Zhang, H. Yan, B. Ying, X. Guo, X. Sun, *Inorg. Chem. Front.* **2023**, *10*, 2100.
[42] Z. Pu, T. Liu, G. Zhang, Z. Chen, D. S. Li, N. Chen, W. Chen, Z. Chen, S. Sun, *Adv. Energy Mater.* **2022**, *12*, 2200293.
[43] R. Zhang, J. Cao, T. Peng, K. Wu, Y. Shu, *Electrochim. Acta* **2024**, *487*, 144166.
[44] Y. Liu, X. Liu, A. R. Jadhav, T. Yang, Y. Hwang, H. Wang, L. Wang, Y. Luo, A. Kumar, J. Lee, H. T. D. Bui, M. Gyu Kim, H. Lee, *Angew. Chem., Int. Ed.* **2022**, *61*, e202114160.
[45] J. Liu, J. J. Hinsch, H. Yin, P. Liu, H. Zhao, Y. Wang, *J. Electroanal. Chem.* **2022**, *907*, 116071.
[46] X. Yin, H. Wang, S. Tang, X. Lu, M. Shu, R. Si, T. Lu, *Angew. Chem., Int. Ed.* **2018**, *57*, 9382.